Proceedings of the 21st ICSMGE, Vienna, Austria, 14 – 19 June 2026. Pistrol, Adam & Schweiger (eds.)
Published by: ÖGG, Austrian Society for Geomechanics, Salzburg, Austria, ISBN 978-3-9503898-4-5
https://doi.org/10.53243/ICSMGE2026-2239

Physical modeling of failure accompanied by near-surface collapse characterizing cyclic soil structure interaction in integral bridges

Dunja Perić
Department of Civil Engineering, Kansas State University, USA, peric@ksu.edu

ABSTRACT: Although absence of deck expansion joints in integral bridges brings multiple benefits, such as increased redundancy and resilience, lower construction costs, and improved vehicular ride quality, the evolving soil structure interaction behind the abutments results in detrimental distress of bridge approach slab that starts very early in the life cycle of the bridge, thus posing a threat to traffic safety and requiring maintenance. This study investigated the complexities of the cyclic soil structure interaction by adopting an experimental approach, in which a downscaled model of the abutment, piles, and backfill was subjected to load cycles simulating the effects of thermally induced expansions and contractions of the bridge superstructure. In addition to contact measurements of load and displacement, a high-resolution digital camera and digital imaging correlation software were used to obtain the strain field in the backfill behind the abutment. The selected magnitude of the abutment top displacement induced three concurrent deformation mechanisms, including two distinct shear bands, internal and interfacial, that were accompanied by the near-surface soil collapse responsible for the bridge approach settlement.

KEYWORDS: Integral bridges, bridge approach settlement, near-surface collapse.

1 INTRODUCTION

Seasonal thermally induced superstructure expansions and contractions in non-integral bridges are accommodated by deck expansion joints that incur additional construction and maintenance costs. In integral bridges (IBs), these superstructure deformations are transferred to the abutments and ultimately to the soil surrounding the abutments and piles through a complex, cyclic soil-structure interaction, resulting in backfill settlement. During winters, abutments move away from the granular backfill, causing the formation of a void directly below the approach slab. Although during summers the superstructure expansion causes abutments to move towards the backfill, the previously formed void persists and grows in size with the increasing number of seasonal temperature cycles, resulting in the loss of contact between the approach slab and backfill, which leads to approach slab distress and settlement. Additionally, the abutment motion may induce active and passive failure in the backfill, depending on the magnitude of displacement experienced by the abutment.

The primary objective of this study was to develop an in-depth understanding of the underlying deformation mechanisms through physical modeling, thereby providing a necessary knowledge for the development of effective mitigation methods. The recent related previous experimental research (Al-Qarawi, 2016; Al-Qarawi, 2021; Liu et al., 2021; Sidgel et al., 2021; Sigdel et al., 2023) used full-size abutments without piles, subjected to translation and/or rotation, while the present study modeled a configuration that more closely resembles the IBs in the U.S., comprising a stub abutment, piles, and granular backfill. The physical model was subjected to loading cycles simulating thermally induced displacements. In addition to contact measurements of force and displacement, a high-resolution digital camera, along with digital image correlation (DIC) software (Peters et al., 1983), was used to capture deformation mechanisms in detail.

2 EXPERIMENTAL SETUP

2.1 *Soil enclosure, abutment and piles*

The physical model was constructed by downscaling a section of the abutment and two piles of the "Bemis Road Bridge: F-4-20" over the Nashua River in Fitchburg, Massachusetts (Perić et al., 2016), five times. The floor of the soil enclosure, constructed from two pieces of plywood, each 1.27 cm thick, measured 1.09 m x 1.50 m. The front wall, through which the abutment is visible in Figure 1, and the back wall were made of 2.54 cm-thick plexiglass, measuring 1.12 m in height and 1.5 m in width. The right and left side walls, measuring 1.12 m in height and 1.14 m in width, were composed of two pieces of plywood, each 1.25 cm thick. The abutment, which was made of an aluminum block measuring 0.483 m in height, 1.09 m in length, and 0.152 m in width, was supported by two hollow aluminum piles with a center-to-center spacing of 0.55 m (Figure 2). Each pile had a diameter of 3.81 cm, a wall thickness of 0.508 cm, and a length of 50.8 cm. Figure 2 shows the abutment along with the attached piles, load cell, and a part of a screw jack. The distance between the center of each pile and the edge of the abutment that is in contact with the plexiglass wall, which is 0.27 m, is considered sufficient for preventing any undesired boundary effects. The load cell and screw jack assembly is attached to the abutment 8 cm below its top. Loading was applied by controlling the rate of horizontal displacement at this elevation. As seen in Figure 1, four steel angles were connected to form a rectangle, thereby providing bracings at the bottom, top, and 0.356 m from the bottom of the container. The additional steel angles connecting two long walls were placed at the top of the container. To produce the desired movement, a screw jack was connected to the reaction frame, which comprised two steel channels extending along the wooden vertical walls (Figure 1). The channels were connected with two long threaded rods extending along the plexiglass walls. In accordance with Meymand (1998), the flexural rigidity of the model piles was scaled at $1/\lambda^5$ with respect to the prototype piles, where λ is a length scale factor, equal to five in this case.

While proper scaling of self-weight stresses is necessary in most soil mechanics applications, it is likely not significant in this case. Firstly, active and passive failures are governed by the magnitude of the horizontal displacement normalized by the abutment height. Secondly, active failure in this case is intrinsically linked to the near-surface collapse of the granular backfill caused by the temporary loss of confinement, which is the primary cause of the backfill settlement. The collapse starts at the ground level and propagates deeper with increasing abutment displacement. Knowledge about the near-surface collapse is scarce, but it is likely that it is affected by the soil gradation, relative density, and the magnitudes of the abutment's rotation and translation. Overall, it is expected that the upscaled settlement observed in these experiments would provide a good estimate of the backfill settlement in the prototype.

Figure 1. Soil enclosure with soil and abutment

Figure 2. Abutment, piles, and load cell

2.2 *Backfill soil*

Kansas River sand, with a mean grain size (D_{50}) of 2.6 mm, was used in this study. Coefficients of uniformity and curvature are 3.18 and 0.9, respectively, and an effective friction angle is 42.2° at a relative density of 75%, based on the minimum and maximum dry unit weights of 16.02 and 18.85 kN/m^3, respectively (Liu et al., 2021). Consequently, the Kansas River sand is poorly graded sand (SP) according to the Unified Soil Classification System (USCS). The sand was placed and compacted at a relative density of 75% in five lifts below the abutment bottom and additional lifts above the abutment bottom. Black aquarium sand was added within about 2 cm of the plexiglass wall facing the camera to provide a sufficient contrast for digital imaging.

2.3 *Control mode*

The experiment was conducted in a displacement control mode, whereby a horizontal displacement amplitude of 0.3 cm was manually applied at the top of the abutment, resulting in a displacement amplitude-to-abutment height ratio of 0.6%. This value was selected based on the prototype ("Bemis Road Bridge") displacement obtained from the computational model (Perić et al., 2016) for the total temperature change of 55.4°C. The prototype bridge is a three-span bridge with a total length of 45.7 m. Thus, the length of the bridge and the magnitude of thermal load are representative of the state of Kansas. Specifically, the horizontal displacement obtained from the computational model was 13.5 mm, which, with the prototype abutment height of 2.44 m, results in a horizontal displacement-to-abutment-height ratio of 0.0056. This value was slightly increased to 0.006 in this study to ensure the likelihood of active failure occurrence.

hus, the ratio of the horizontal displacement and abutment height in the model is equal to the one corresponding to the prototype ("Bemis Road Bridge").

3 RESULTS

This paper focuses on the first five loading cycles because the approach slab distress begins very early after the bridge construction is completed. 3 shows the photograph of the deformed configuration at the beginning of the fifth cycle, after the abutment was moved 3 mm away from the backfill. The data acquisition system was capable only of logarithmic time sampling, resulting in the most complete data for each tenth cycle.

Figure 3. Beginning of the fifth cycle

Figure 4 depicts the total horizontal force acting on the abutment vs. the horizontal displacement, both measured 8 cm below the top of the abutment, thus indicating that the maximum force increased while the change in the minimum force is negligible. Compressive force is positive while tensile force is negative, and displacement away from the backfill is positive. The total force includes the earth pressure and the friction force acting between the abutment and the plexiglass walls.

Figure 5 shows the evolution of total and incremental settlement at the interface of the abutment and backfill during the first five cycles. The final total settlement was 15 mm, while the largest incremental settlement in the amount of 5.7 mm occurred at the end of the first cycle.

Figure 6 depicts the settlement profile at the end of the fifth and 10th cycles. At the end of the first cycle, the settlement extended horizontally up to a maximum distance of 250 mm from the interface, corresponding to 51.7% of the abutment's height. The settlement profile after 10 cycles is provided for comparison, showing that the lateral extent of settlement at this time has increased to 300 mm, or 62.1% of the abutment height. This indicates that the void behind the abutment increases in size with the increasing number of load cycles. The void is located below the approach slab in IBs, but the approach slab is not included in the physical model employed herein. The lateral extent of settlement represents the unsupported length of the approach slab that becomes significant even after only five loading cycles, likely leading to the early development of approach slab distress. The larger the void created by settlement, the more extensive and time-consuming the mitigation efforts required.

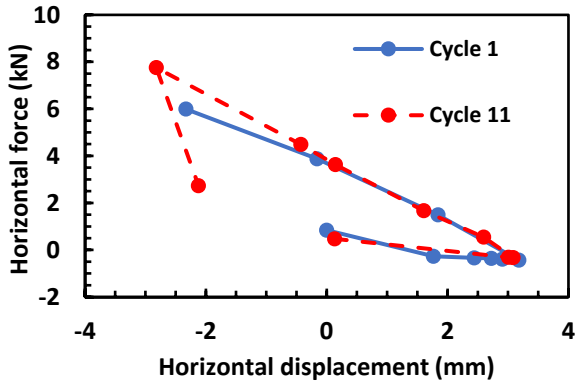

Figure 4. Horizontal force vs. horizontal displacement.

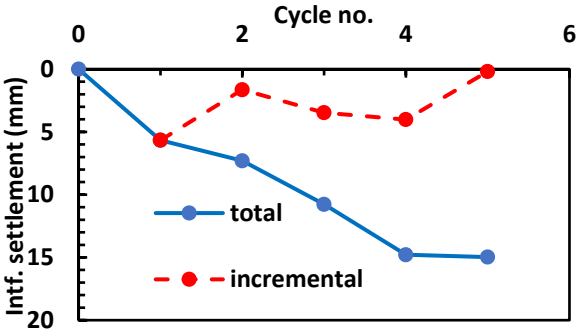

Figure 5. Backfill settlement at interface vs. cycle number.

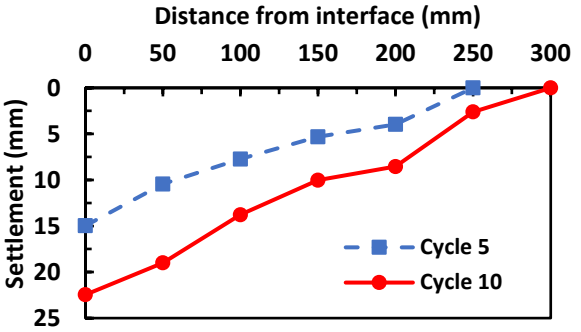

Figure 6. Lateral extent of backfill settlement.

To further elucidate the underlying deformation and failure mechanisms responsible for the evolution of backfill settlement, Lagrangian in-plane shear strains were obtained by using DIC software VIC-2D. Figure 7 and Figure 8 show Lagrangian shear strain fields after the abutment moved 3 mm away from the backfill, at the beginning of the first and fifth cycles, respectively.

Figure 7 shows that localized deformation developed within two distinct shear bands already after the abutment moved 3 mm away from the backfill for the first time. While the internal shear band, which indicates active failure, does not extend to the ground surface, it is clearly present and significantly long. The corresponding maximum magnitude of shear strain is about 1%. Another shear band develops along the interface of the abutment and backfill, featuring the maximum magnitude of shear strain of about 0.7% that occurs closer to the ground level, thus indicating that corresponding localized deformation is caused by the falling of sand particles in the gap between the abutment and backfill. There might have been some local interference of the strain in the steel rod with the overall strain field, but digital imaging still successfully captures the main features of the relevant deformation mechanisms in the backfill soil.

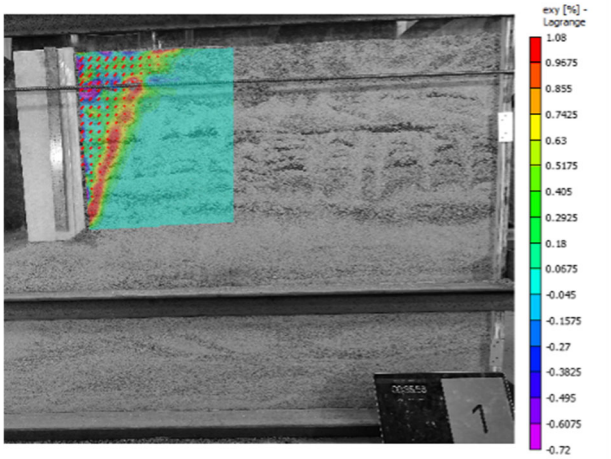

Figure 7. Lagrangian shear strain (%) at the beginning of the 1st cycle.

Figure 8 shows Lagrangian shear strain after the abutment moved 3 mm away from the backfill at the beginning of the fifth cycle. The internal shear band is somewhat shorter than in Figure 7, but still present. Shear strain within this shear band is more non-uniform than at the beginning of the first cycle, with the maximum magnitude of about 5%. Although the interface shear band is still present it is not continuous, and the maximum shear strain occurs exactly in the region from where sand moves into the gap created by the movement of the abutment away from the backfill. The maximum magnitude of shear strain in this region is about 3.25 %.

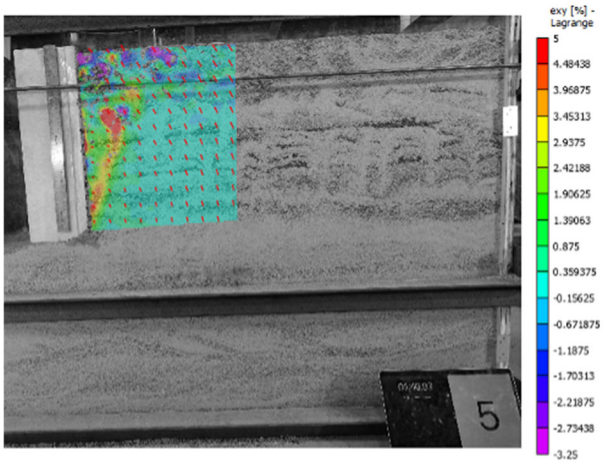

Figure 8. Lagrangian shear strain (%) at the beginning of the fifth cycle

Digital imaging has also captured localized deformation that develops below the tip of the LVDT used to measure vertical soil surface displacement, both in Figure 7 and Figure 8.

Comparison of Figure 7 and Figure 8 shows that the magnitude of localized shear strains increases with progression of loading cycles, five-fold in the internal shear band and 4.22 times at the interface, over five loading cycles. Consequently, the increase in size of the void that forms behind the abutment and below the approach slab is accompanied by the growth of localized deformation within the internal shear band and at the interface between the abutment and backfill. Even in the case that active failure does not occur, which is unlikely due to the

small amount of displacement that it requires, the near-surface backfill collapse would occur simply due to the inability of cohesionless soil to follow the outward motion of the abutment.

4 CONCLUSIONS

The experiment simulating the cyclic thermally induced motion of the IB's stub abutment, surrounded by backfill and supported by piles, was performed on the downscaled model in displacement control mode. Contact measurements, along with high-resolution photographs and the use of DIC software, provided excellent insight into the underlying deformation and failure mechanisms relevant to the bridge approach settlement and approach slab distress.

The cyclic abutment motion away from the backfill produced a cyclic temporary lack of confinement, thereby causing a near-surface collapse of the cohesionless backfill within the limited region directly behind the abutment. The collapse led to the formation of a void that grew with every additional movement of the abutment away from the backfill. Thus, the temporary lack of confinement causes instability, leading to a collapse that manifests itself in the surface settlement. In this study, the amplitude of the abutment displacement, which was 3 mm, caused active backfill failure, manifesting as a corresponding persistent shear band. Another, more erratic shear band formed at the interface of the abutment and backfill, indicating that collapsed soil particles were falling into this region.

In summary, the research results presented herein indicate that successful mitigation methods must suppress or decrease the amount of confinement loss in the near-surface region of the backfill, caused by the outward motion of the abutment. Mitigation methods may include the use of different forms of geosynthetics, either alone or in combination with geofoam blocks, in configurations that provide persistent confinement to the backfill. The efficiency of a selected mitigation method can be quantified by measuring the progress in lateral extent of settlement and void size with increasing number of loading cycles.

5 ACKNOWLEDGEMENTS

The author would like to acknowledge the support of the Kansas Department of Transportation for this research, received through the KTRAN program.

6 REFERENCES

Al-Qarawi, A. 2016. *The application of EPS geofoam in mitigating the approach problems in integral abutment bridges*. Master's thesis. Western Sydney University.

Al-Qarawi, A. 2021. *A study on the fundamental behavior of soil-structure interaction and mitigating effects of EPS geofoam inclusions in integral abutment bridge*. Ph.D. thesis. Western Sydney University.

Liu, H., Han, J., and Parsons, R. L. 2021. Mitigation of seasonal temperature change-induced problems with integral bridge abutments using EPS foam and geogrid. *Geotextiles and Geomembranes*, 49(5), 1380-1392.

Perić, D., Miletić, M., Shah, B. R., Esmaeily, A., and Wang, H. 2016. Thermally induced soil structure interaction in the existing integral bridge. *Engineering Structures*, 106, 484-494.

Meymand, P.J. 1998. *Shaking Table Scale Model Test of Nonlinear Soil-Pile-Superstructure Interaction in Soft Clay*. PhD thesis. University of California, Berkley.

Peters, W. H., Ranson, W. F., Sutton, M. A., Chu, T. C., and Anderson, J. 1983. Application of digital correlation methods to rigid body mechanics. *Optical Engineering*, 22(6), 738-742.

Sigdel, L. D., Leo, C. J., Liyanapathirana, S., and Hu, P. 2021. Integral bridge abutment-soil interaction analysis using PIV technique. *Proc. of the International Conference on Geotechnical Engineering, ICGE-Colombo-2020: Geotechnics in a Challenging Environme*nt, Colombo, Sri Lanka, 253-258.

Sigdel, L. D., Lu, M., Al-Qarawi, A., Leo, C. J., Liyanapathirana, S., and Hu, P. 2023. Application of engineered compressible inclusions to mitigating soil-structure interaction issues in integral bridge abutments. *Journal of Rock Mechanics and Geotechnical Engineering*, 15(8), 2132-2146.